


# Effect of reservoir geometry on vortex trapping of cancer cells

P. Paiè<sup>1</sup>  · J. Che<sup>2,3</sup> · D. Di Carlo<sup>2,3,4,5,6</sup>

Received: 6 April 2017 / Accepted: 27 May 2017 / Published online: 2 June 2017  
© Springer-Verlag Berlin Heidelberg 2017

**Abstract** Vortex-aided particle separation is a powerful method to efficiently isolate circulating tumor cells from blood, since it allows high throughput and continuous sample separation, with no need for time-consuming sample preprocessing. With this approach, only the larger particles from a heterogeneous sample will be stably trapped in reservoirs that expand from a straight microfluidic channel, allowing for efficient particle sorting along with simultaneous concentration. A possible limitation is related to the loss of particles from vortex traps due to particle–particle interactions that limit the final cellularity of the enriched solution. It is fundamental to minimize this issue considering that a scant number of target cells are diluted in highly cellular blood. In this work, we present a device for size-based particle separation, which exploits the

well-consolidated vortex-aided sorting, but new reservoir layouts are presented and investigated in order to increase the trapping efficiency of the chip. Through simulations and experimental validations, we have been able to optimize the device design to increase the maximum number of particles that can be stably trapped in each reservoir and therefore the total efficiency of the chip.

**Keywords** Inertial microfluidics · Size-based separation · Vortex-aided sorting · Trapping stability optimization

## 1 Introduction

Circulating tumor cells (CTCs), first observed in 1869 (Ashworth 1869), are cancerous cells that travel in the blood, disseminated from tumor foci in tissue. These cells have a predominant role in metastasis formation, and it is extremely important to study their properties to better understand metastasis development, which causes ~90% of tumor-related deaths (Pantel and Alix-Panabières 2010). Moreover, the concentration of these cells in blood reveals the aggressiveness of the tumor and may provide insight into the ongoing treatment response of the patient. For this reason, counting these cells serves as a liquid biopsy which can have a high impact on cancer monitoring, substituting more invasive and time-consuming methods (Alix-Panabières and Pantel 2013). Another aspect that determines CTC importance is the possibility to develop personalized cancer therapies (Riethdorf et al. 2010; Paris et al. 2009). Indeed, recently innovative targeted cancer therapies have been used, where patients are exposed to drugs against specific molecular lesions. These drugs are developed on the basis of the molecular analysis of the tumor; nevertheless, the primary tumor may be inaccessible or may have

---

✉ P. Paiè  
petra.paiè@mail.polimi.it

<sup>1</sup> Istituto di Fotonica e Nanotecnologie (IFN)-CNR and Dipartimento di Fisica, Politecnico di Milano, Piazza Leonardo da Vinci 32, 20133 Milan, Italy

<sup>2</sup> Department of Bioengineering, University of California, Los Angeles 420 Westwood Plaza, 5121 Engineering V, Los Angeles, CA 90095, USA

<sup>3</sup> Vortex Biosciences Inc., 1490 O'Brien Drive, Suite E, Menlo Park, CA 94025, USA

<sup>4</sup> Department of Mechanical Engineering, University of California, Los Angeles 420 Westwood Plaza, 5121 Engineering V, Los Angeles, CA 90095, USA

<sup>5</sup> California NanoSystems Institute, University of California, Los Angeles 570 Westwood Plaza, Los Angeles, CA 90095, USA

<sup>6</sup> Jonsson Comprehensive Cancer Center, University of California, Los Angeles 10833 Le Conte Ave, Los Angeles, CA 90024, USA

already been surgically removed. Moreover, it is important to remember that often mutational differences between the primary tumor and metastasis can occur. For these motivations, the isolation and analysis of CTCs can furnish a more complete description of the metastatic progression, to better indicate the effectiveness of a targeted therapy. Much is still possible to discover about CTC properties, but due to their fundamental role in cancer progression the analysis of these cells is extremely promising.

The main limitation to these studies is related to the technical difficulties that have to be faced to successfully isolate these cells, due to their extreme rarity. Indeed, there are often only a few CTCs per mL of blood, diluted in billions of red blood cells and millions of white blood cells. Several technologies have been proposed so far (den Toonder 2011). The quality of these methods depends on (1) the efficiency in isolating cells, (2) the purity of the isolated subpopulation, which can still contain trace red and white blood cells and (3) the speed of the procedure, which is fundamental to make CTC isolation an effective alternative to standard biopsy. Microfluidic platforms have shown particular promise to these ends (Chen et al. 2012).

The existing isolation methods separate CTCs using their biological (specific surface protein expression) or physical properties (such as size, deformability, dielectric properties, density and optical properties). The majority of approaches utilize immunomagnetic separation, in which magnetic beads selectively attach to CTCs using a coating of antibodies specific for the cell type, such as the use of anti-EpCAM (Epithelial Cell Adhesion Molecule)-conjugated microparticles. On this principle is based the Cell-search system (Janssen Diagnostics, LLC), which is commercially available and so far the only approach approved by the US Food and Drug Agency (FDA) (Riethdorf et al. 2007) for CTC enumeration for patient prognosis evaluation. But the capture efficiency is still low, and the measurement requires cell fixation, preventing further analysis requiring viable cells for the isolated sample. Moreover, the biological separation approach risks neglecting the large CTC heterogeneity, in fact the efficiency of this approach is based on EpCAM expression, which not only varies among different cancer types but also can change over cancer progression in the same patient.

Great benefits in terms of purity and throughput arise from the use of microfluidic platforms, where the precise flow control permits high-efficiency cell sorting and rapid flows enable fast sample processing rates (Li et al. 2013). Different approaches have been so far implemented: typical examples of biological sorting make use of magnetic-based CTC separation and cell affinity chromatography. The first one uses antibody–antigen interactions to bind magnetic particles to a cell, and through a magnetic field it performs the cells isolation (Hoshino et al. 2011).

The mean throughput (10 ml/h) and the efficiency of this method are quite good, but on the other side the necessity of cell pretreatment and the lack of cell viability represent the main drawback of this approach. Cell affinity chromatography (Stott et al. 2010; Nagrath et al. 2007) still uses an antibody–antigen interaction, but in this case the target cells bind to antibody-coated surfaces, preventing the need of a labeling step required in the previous method. Lower throughput and more complex device layout are required, in order to favor cell interactions with coated surfaces and to reduce the shear stress which could detach cells from coated surfaces. Dielectrophoretic separation approaches (Gupta et al. 2012) use non-uniform dielectric fields to induce a dielectric force over particles which is dependent on the particle's properties and therefore it allows selective cell isolation with no need of sample labeling step, high cell viability (up to 97%) and reasonable sample throughput are demonstrated (1 ml/h). Alternatively, size-based methods, which exploit the difference in dimension between CTCs and the smaller blood cells, are particularly promising since they do not require antibodies and sample preprocessing, they are cost-effective, and they permit continuous sample separation (Kim et al. 2012; Zheng et al. 2007; Lin et al. 2010). Filter-based devices belong to this category, but due to the high deformability of these cells that can pass through filter pores this approach is not very efficient; moreover, even though this is a simple approach, the risk of clogging when working with non-diluted samples is limiting. To overcome this limitation, Yeo et al. (2016), instead presented a device, which combines hydrodynamic focusing and active chambers, which permit to trap or release the isolated cells, avoiding the main channel clogging. Rare cell isolation from white blood cells has been carried with very high purity, but to process about 100'000 cells up to 3 h can be required. Some interesting microfluidic devices have been presented with sorting capabilities based on both fluid properties and cell dimensions, which leads to a physical separation of cells by size (Geislinger and Franke 2013; Louterback et al. 2012; Bhagat et al. 2011; Lee et al. 2013; Pødenphant et al. 2015; Sollier et al. 2014). Often the purity and the throughput that can be obtained are a compromise, but it is particularly interesting that some of these technologies exploit inertial effects of the fluid, obtaining efficient separation at high flow rates, simply exploiting the microchannel layout, with no need of any active field that could affect the sample viability. For example, Warkiani et al. 2014 present a spiral microchannel to efficiently isolate CTCs from blood thanks to the superposition of inertial lift forces and Dean drag. Good efficiency and high throughput ( $\approx 1$  ml/min) characterize this device, but also additional steps of centrifugation might be required downstream to reduce the collected sample dilution and to perform downstream assays. Ozkumur et al. (2013) presented

the CTC-iChip device, which by exploiting the sequence of deterministic lateral displacement, inertial particle focusing and magnetic positive or negative depletion managed to separate CTCs at high throughput (8 ml/h), with good efficiency and high cell viability. Nevertheless, the complexity of this device, the low purity of negative depletion (0.1%) and the antibody requirements are still open issues to face. A different approach is the one used in the Vortex chip, based on a series of microchannel expansions (named reservoirs), dislocated along a straight channel, that allow to selectively trap larger particle. This method permits size-based sample separation with high purity, good efficiency, fast processing time and without affecting the cell viability (Sollier et al. 2014; Dhar et al. 2015). Moreover, with this technology no centrifugation step is needed, allowing collection of target cells directly in a small liquid volume. In this work, we focus on new device layouts, to further increase the trapping efficiency of Vortex chips and to reduce the instability due to the simultaneous presence of several particles in each reservoir.

## 2 Vortex technology

A recently proposed device from the Di Carlo group is the Vortex chip (Sollier et al. 2014; Che et al. 2013), capable of extracting CTCs from blood samples with high efficiency and purity. The device, which is fabricated in a PDMS substrate with soft lithography, relies on inertial effects, for which hydrodynamic forces act on particles and manipulate

their position in the channel on the basis of their size. The device schematic is reported in Fig. 1, which consists of straight parallel channels along which a series of larger rectangular reservoirs are evenly distributed.

Particles flowing in the straight channels tend to migrate away from the channel centerline due to the presence of inertial lift forces that act on the sample at relatively high flow rates (the sample is infused at about 500  $\mu\text{l}/\text{min}$  in each channel) (Di Carlo 2009). Indeed, if the particle Reynolds number ( $\text{Re}_p$ ) is about 1 or larger, two counteracting forces act on the particles.  $\text{Re}_p$  is equal to  $\text{Re} (a/W_c)^2$ , where  $a/W_c$  is the particle dimension over the channel dimension.  $\text{Re}$  is the channel Reynolds number which is equal to  $\rho U_m D/\mu$ , with  $\rho$  equal to the fluid density,  $U_m$  the maximum velocity, and  $\mu$  the dynamic viscosity. The first force is the shear gradient lift force  $F_S$  equal to  $f_{Ls} U_m^2 a^3/W_c$ , where  $f_{Ls}$  is the dimensionless lift coefficient. This force tends to push particles away from the center of the channel, due to the shape of the parabolic velocity profile. A wall-effect lift force ( $F_W$ ) acts in the opposite direction displacing the particles from the walls and is equal to  $f_{Lw} U_m^2 a^6/W_c^4$ , where  $f_{Lw}$  indicates the related dimensionless lift coefficient.

Figure 1 shows particles migrating toward the wall before entering the reservoirs, where at sufficiently high flow rates fluidic vortices are formed. Once the particles reach the expansion region, the wall-effect force diminishes, while the shape of the velocity field decays slowly with downstream distances such that the shear gradient lift force contributes predominantly to the particles position.

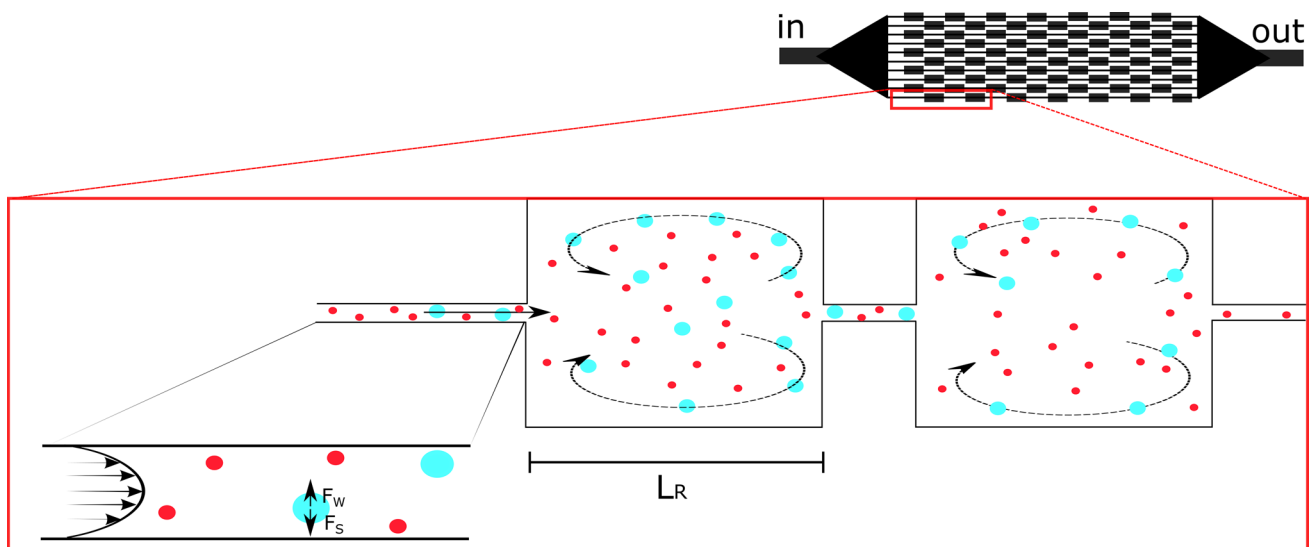


**Fig. 1** Scheme of the Vortex chip. Large particles (blue circles) in rectangular straight channels migrate toward the walls. This facilitates the trapping effect of the vortices that originate in the reservoirs. Larger particles experience higher shear gradient forces and can be

stably trapped, while smaller particles flow out of the vortices. Black arrows indicate flow direction.  $L_R$  is the length of each reservoir, equal to 720  $\mu\text{m}$ . The width of the main inlet channel is 50  $\mu\text{m}$  (color figure online)

Since this force depends on the radius of the particle, the larger ones enter into the reservoir, where a vortex is formed, and are stably entrapped by the shear gradient lift that is directed to the vortex center. This permits trapping of larger particles/cells, while smaller particles flow outside the vortex or are not stably trapped. After the sample is processed, the flow rate may be lowered to permit a rapid release of all the trapped cells.

The efficiency of the device depends on the flow rate and the number of reservoirs in series. Indeed, the larger the number of vortices, the higher the possibility that a cell is trapped, while the parallelization permits the reduction of the fluidic resistance and processing of more sample simultaneously. The device efficiency depends also on the reservoir saturation, and this saturation is due to the fact that each reservoir can stably host a maximum number of particles, after which the interaction of particles causes unstable entrapment which may hinder device performance, as discussed by Haddadi and Di Carlo (2017). Unfortunately, it is not possible to add too many reservoirs in series because the longer the channel the higher the fluidic resistance, and the higher pressure required to drive flow can lead to delamination of microfluidic devices, so that a long channel can be unable to sustain the necessary flow rate. Moreover, not too many channels in parallel can be added; otherwise, the flow rate at the inlet of the device will be too high, causing shearing of the sample and device delamination. Another important aspect is related to the blood dilution. Indeed, the presence of billions of red blood cells flowing in the device influences the trapping stability of target cells. Even if the red blood cells are not stably trapped, they may flow through the vortices, interacting with the cells in the traps and altering the stability of these cells.

These concrete problems limit device efficiency. In this work, different reservoir geometries are explored in order to increase the device efficiency without affecting the chip dimensions, and to develop a device where particle–particle interactions play a more minor role on the device efficiency, which is fundamental in blood sample processing. The new geometry layout is partially inspired from the work of Wang and Papautsky (2015), where the presence of side outlets from the reservoirs permits extraction of the trapped particles while processing the sample, with the advantage that particle collision does not affect the trapping stability. This interesting method, unfortunately, is not compatible with the Vortex chip layout, due to the presence of the side outlet channels that prevent the possibility to pack many reservoirs in a compact footprint, which detrimentally affects the total sample processing time. In addition, non-continuous separation in the Vortex technology has the advantage of also concentrating the isolated sample of cells in a smaller volume. The geometry we propose

originates from the idea of maintaining the layout of the Vortex chip, while still trying to reduce the impact of particle collisions. With this regard, we have introduced side channels to the standard reservoirs, which split the fluid stream lines, influencing the path of the cells trapped in the vortex and allowing some of the cells to flow in this lateral fluidic circuit, which sequesters cells over many cycles of the main vortex. We expect the main advantage to be related to the possibility to stably host in a single reservoir more particles without being affected by particle collision. An example of the new geometry is reported in Fig. 2, where lateral channels (colored in yellow in the schematic image) are added to the normal footprint of the vortex reservoir and joined through a connection channel (colored in red), that permits the recirculation of the fluid in this area of the reservoir. In this work, different geometries, similar to the one reported in Fig. 2, are proposed and their trapping efficiency is compared with the standard Vortex chip. Different lengths of the lateral channels ( $\alpha$ ) and widths of the connection channel ( $\beta$ ) are explored, to find out the configuration that permits optimal device efficiency. In this work, the efficiency measurements are performed with 20  $\mu\text{m}$  beads as a reference sample, and comparing the different results we aim to optimize the trapping stability. Note that it is also possible to optimize the single reservoir geometry, as reported by Dhar et al. (2015), to trap more efficiently smaller particles, but at the price of a reduced purity.

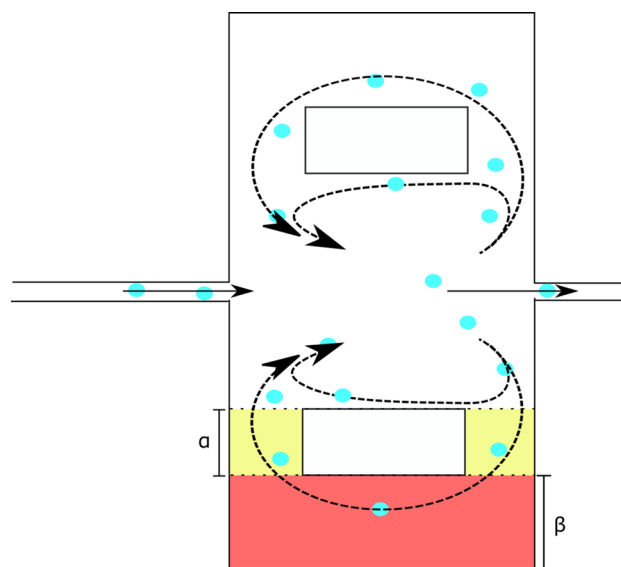


**Fig. 2** Schematic layout of a new reservoir geometry. Lateral channels (in yellow) are added to the standard reservoir footprint, which are joined with a connection channel colored in red. Different lengths of the lateral channel ( $\alpha$ ) as well as the width of the connection channel ( $\beta$ ) are explored. Arrows indicate the fluid stream lines. Blue circles indicate cells (color figure online)

### 3 Materials and methods

#### 3.1 Device fabrication

The devices studied in this work are fabricated by soft lithography in a PDMS substrate and plasma-bonded to a glass slide. The standard Vortex chip consists of ten parallel channels 36 mm long, with a series of 12 reservoirs along each channel and separated by 1 mm. The straight channel between reservoirs is 50  $\mu\text{m}$  wide and 70  $\mu\text{m}$  in height, and the reservoirs are 720  $\mu\text{m}$  long and 245  $\mu\text{m}$  wide on each side and 70  $\mu\text{m}$  in height. Different geometries are investigated, maintaining the same basic footprint, but adding to each reservoir two channels joined by a connection channel. Different dimensions are explored in order to maximize the device trapping efficiency.

#### 3.2 Capture efficiency measures

The capture efficiency experiments are performed by diluting a known percentage of beads in the solution that is then processed through the device. Each device has two inlets in series: one is used to infuse the sample, and one just the buffer solution which is normally used to wash the residual red blood cells before releasing the trapped cells. Syringe pumps (Harvard Apparatus PHD 2200) are used to deliver the sample through the chip at precise and high flow rates. The device is placed on a standard inverted microscope, and during the experiments a high-speed camera permits observation of the sample during capture (Phantom V711, with minimum integration time of 1  $\mu\text{s}$ ). PEEK tubing is inserted in the chip and connected to the syringes (the inlets) and to the waste (the outlet). During the measurements, the flow rate in each channel, which was previously optimized, is kept equal to 500  $\mu\text{l}/\text{min}$ . Considering that the chip is made by 10 distinct channels, a total flow rate of 5 ml/min is imposed. The measurement procedure consists of:

1. Vortex formation: buffer is flowed at high flow rate, to enable vortex formation, which takes several seconds.
2. Sample processing: the sample is infused at the same flow rate previously used for the buffer, which is now switched off.
3. Washing step: when sufficient sample is processed, the sample flow is promptly stopped and the buffer is infused without altering the flow rate in the chip.
4. Sample collection: after about 30 s, the flow rate of buffer is decreased and the cells are released from the reservoirs and collected in a 96 well plate.

5. Data averaging: for each experimental condition, at least three measurements are performed, to average the data.

At least three reference wells are filled with the same concentration of particles which is used to obtain the sample solution. The counting is performed using dedicated software on a Zeiss fluorescence microscope (Zen). The software is capable of automatically counting the fluorescent particles in the selected plates. Reference and collection wells are analyzed, and particles are counted to retrieve the efficiency of capture for the experiments. Efficiency is a percentage defined as the number of target particles collected in the well plate over the total number of target particles infused.

#### 3.3 Sample preparation

The beads used (Phosphorex) have a dimension of 20  $\mu\text{m}$  and contained a fluorophore with orange fluorescence. About 300 beads are diluted in 6 ml of deionized water to compare the efficiency of the different devices. Higher sample concentrations have also been used to test the device properties at different conditions.

1- $\mu\text{m}$  fluorescent beads are used to characterize the vortex shape, exploiting the capability of small particles to follow the stream lines without being trapped in the vortices. For these measurements, a long camera exposure time of about a few seconds was used.

### 4 Results and discussion

The new Vortex chip layout is designed to increase the number of particles that can be trapped in a single reservoir, doubling the area of trapped particles trajectories. Indeed, the fact that particles can flow not only in the main vortex, but also in a lateral and more protected path, was hypothesized to allow more beads to be stably hosted in a single reservoir, due to the reduced influence of particle collisions on the device trapping efficiency. Since the device dimensions highly influence the fluid properties, it is important to optimize them to facilitate a balanced splitting of the particles to the two paths, allowing circulation in the lateral channel and in the main vortex at the same time.

We expect that the choice of the lateral fluidic circuit resistance highly influences the preferred particle path; a lateral path characterized by a high fluidic resistance favors the particle circulation in the main vortex; in contrast, we expect that a reduced fluidic resistance tends to facilitate the choice of the lateral path.

In Fig. 3, examples of the two opposite fluidic resistance situations show the disparate results on particle



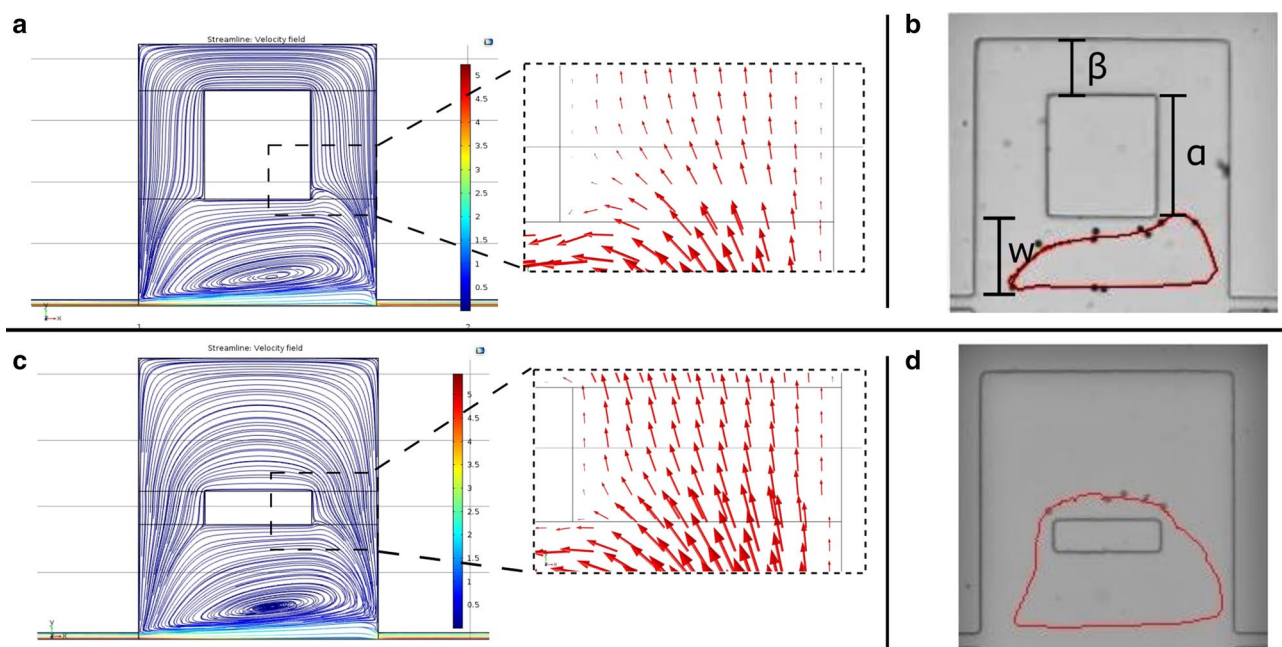


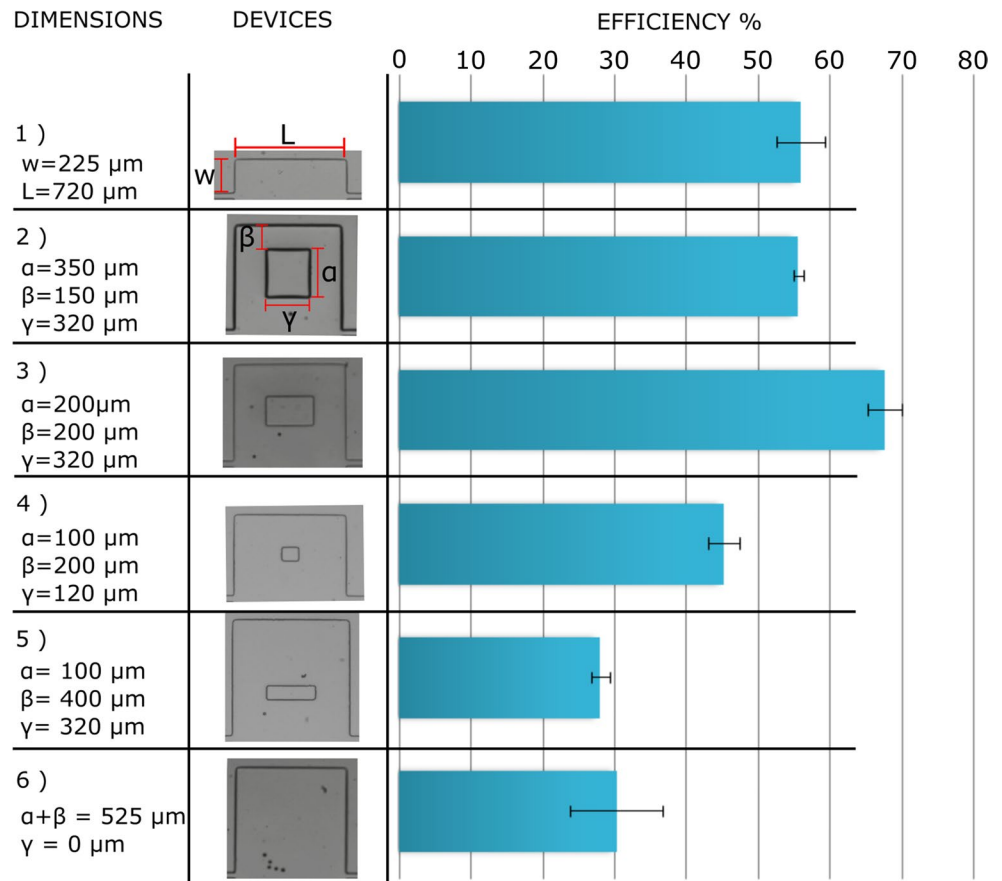
**Fig. 3** Fluid simulations and the particle trajectory analysis of two reservoirs with different side channel dimensions. In *panel a* and *b*, the length of the side channel ( $\alpha$ ) is equal to 350  $\mu\text{m}$ , while the width of the connection channel (*b*) corresponds to 150  $\mu\text{m}$ . In *panel*

*c* and *d*, the same parameters are equal to 100 and 400  $\mu\text{m}$ , respectively. The width of the main vortex chamber ( $w$ ) is maintained equal to 225  $\mu\text{m}$ . The particle trajectory analysis shows the influence of the side channel dimensions on the trapped particle path

orbits: for each case, the Comsol simulation of the fluid streamlines (panels a and c) and the corresponding particle trajectory are reported (panels b and d), showing a good agreement between the two. More in detail, panel a shows the study of the reservoir geometry with the higher fluidic resistance lateral path. The long lateral channels ( $\alpha = 350 \mu\text{m}$ ) are joined by a thin connection channel ( $\beta = 150 \mu\text{m}$ ), which is expected to highly favor the particles to flow in the main vortex. Panel c instead reports the opposite situation, where the lateral path is characterized by short lateral channels ( $\alpha = 100 \mu\text{m}$ ) and a wide connection channel ( $\beta = 400 \mu\text{m}$ ) which permits a reduction in the associated resistance. The Comsol simulations show the fluid streamlines in the two reservoirs and an arrow plot of the velocity field. From these simulations, we have been able to estimate the different fluid flow rates in the two side channels, which is 0.192  $\mu\text{l/s}$  in the first case (panel a) and almost the double in panel c (0.343  $\mu\text{l/s}$ ). This is expected to influence particle orbit behavior; as we have been able to verify using a custom particle tracking software to analyze the videos acquired during the experimental device characterization, the trapped particle trajectory in the two devices is indeed extremely different. In the first device, as shown in panel b, particles are circulating only in the main vortex reservoir, while in panel d the particles are flowing in the secondary path only.

From these considerations, we expect that intermediate values of  $\alpha$  and  $\beta$  must be preferred to obtain a balanced splitting of the particles in the two trajectories and subsequently to enhance the number of particles that can be contained in each reservoir. To better optimize these dimensions, we fabricated different devices covering a wide range of layouts, and in each case we measured the corresponding trapping efficiency. In Fig. 4, the comparison of the different device efficiencies, performed at 5 ml/min, of the most significant examples is reported and these values are compared to the standard Vortex chip efficiency (device number 1). It is interesting to note that the device number 2, which was previously analyzed in Fig. 3 panels a and b and does not favor the circulation in the lateral channel, presents a trapping efficiency equal to the one of the standard Vortex chip, which means that basically no significant improvement occurs due to the presence of the lateral channels, as we were expecting from the previous discussion. Furthermore, device number 5, which is analyzed in Fig. 3 panels c and d, presents a lower capture efficiency, and it is worth noticing that it is comparable to device number 6 which is simply obtained with a larger reservoir and no lateral channels. Indeed, both cases display similar particle trajectories, characterized by a larger vortex shape, which is less efficient in trapping particles with respect to the standard Vortex chip. Device number 4 tests the effect of the  $\gamma$  value presenting a shorter gap combined with an

**Fig. 4** Trapping efficiency of each device performed at 5 ml/min. It is interesting to note that the highest value is obtained with device number 3, which traps 67% of the processed particles, 19% higher than the value obtained for the standard Vortex chip



intermediate  $\beta$  value: in this case, the measured efficiency is still smaller with respect to the standard chip, but higher than the device number 5, indicating that the majority of the particles are still circulating in the lateral path, which has a lower trapping efficiency. It is interesting to note that the highest efficiency measured is obtained with the device number 3, whose lateral path is characterized by intermediate dimensions with respect to the ones analyzed in Fig. 3. This device traps 67% of the inserted particles in a single pass, and this value corresponds to a 19% increase with respect to the efficiency of the standard Vortex chip, equal to 56%. We tried to further enhance the maximum device efficiency by slightly changing the dimensions of the lateral path of device 3, but we did not obtain any significant improvement; for this reason, we maintained these values for a deeper device characterization.

Observing the trajectory of the particles trapped in the reservoirs, we noted that this device behaves as expected. Indeed, some of the beads circulate in the lateral channels, while others remain in the main vortex chamber. Thus, a balanced splitting of the beads on two separate paths is correlated with increased trapping efficiency. This is potentially caused by reducing the trapping instability due to reduced interparticle interactions for particles on different paths, while still maintaining the original vortex shape near

the channel region. Figure 5a shows a microscope image of the beads flowing in one of the reservoirs of the new device, where it is possible to note how some of them flow in the lateral channels, while other stays in the main vortex. The corresponding microscope image of the fluid streamlines is reported in Fig. 5b, which shows that the main vortex still occurs in the main chamber as it happens with the standard Vortex chip, but the stream line splitting allows for circulation in the lateral channel.

We subsequently compared the shape of the main vortex in the new chip with respect to the standard one. Particle trajectories and Comsol simulation, reported in Fig. 6, are in good agreement, showing that the shape of the main vortex is only slightly different in the two devices. Indeed, we can observe that the main vortex shape is a bit larger in the new chip, which also positively influences the stability of the particles in the chamber. This limits the risk of particles being physically pushed out of the reservoirs due to reciprocal interactions.

Since we are expecting that the main impact of the new geometry is related to the increased stability and to the possibility of hosting more particles in a single reservoir, we performed efficiency tests by processing an increasing number of beads. The obtained results are shown in Fig. 7a. The test is performed diluting about 300, 700

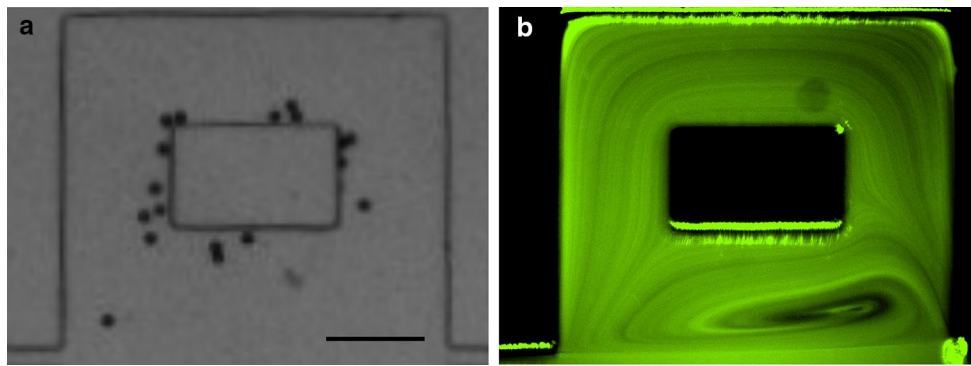


**Fig. 5** Panel a shows the microscope image of the chip with 20- $\mu\text{m}$  beads captured in the reservoir. Some of them are flowing in the main vortex chamber, while others are flowing through the lateral channels. Panel b shows the corresponding fluid *stream lines*. Scale bar is 200  $\mu\text{m}$

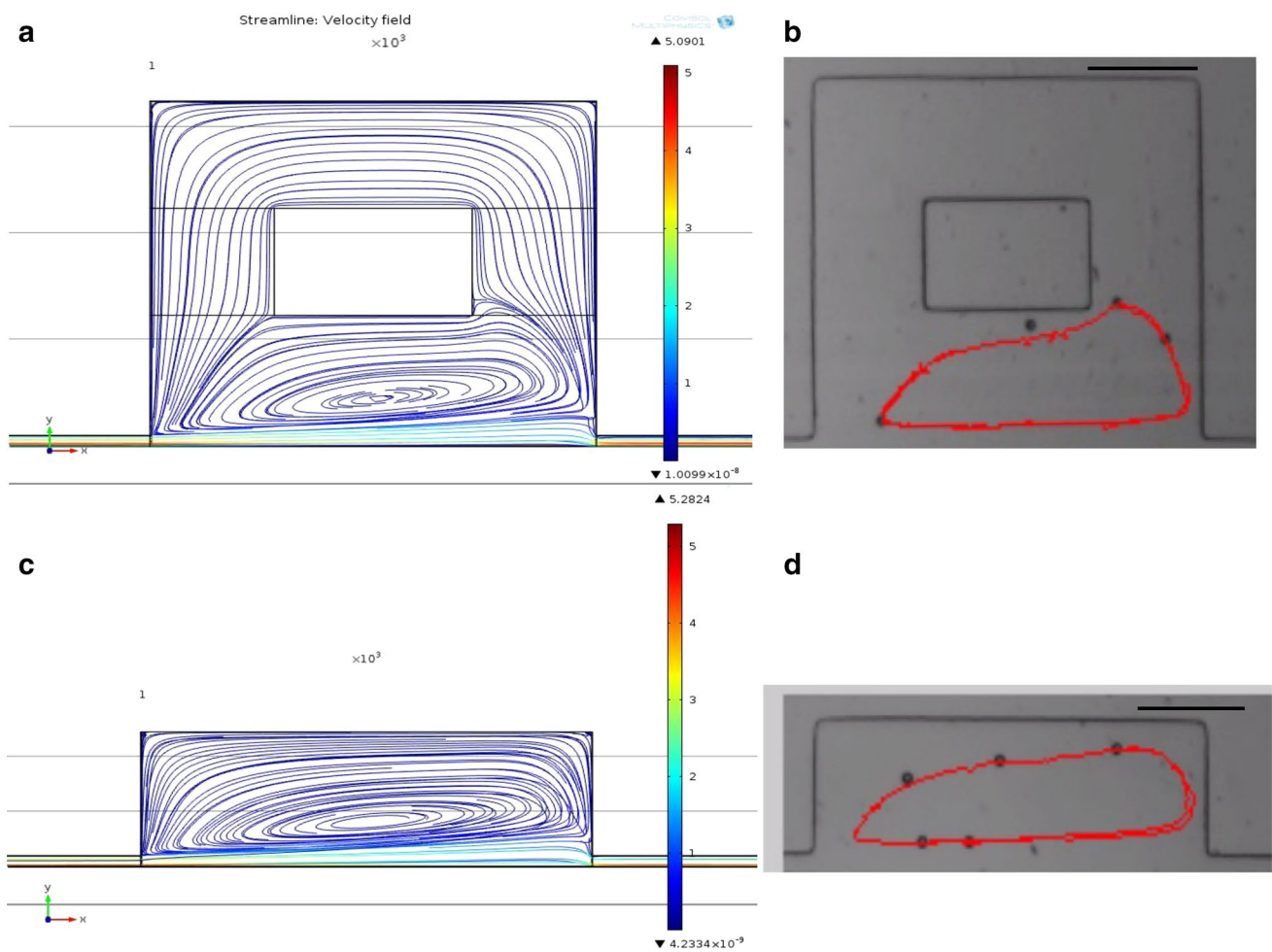


**Fig. 6** Panels a and c show the Comsol simulation of vortex formation in the two devices, while panels b and d show the corresponding particle trajectory. Scale bar is 200  $\mu\text{m}$

and 800 beads in 6 ml of deionized water. It is interesting to note that, as expected, the new device always presents a higher efficiency with respect to the standard chip. But

surprisingly, it seems to saturate before the Vortex chip. Between 700 and 800 beads infused, the new device shows no difference in the number of collected beads, while



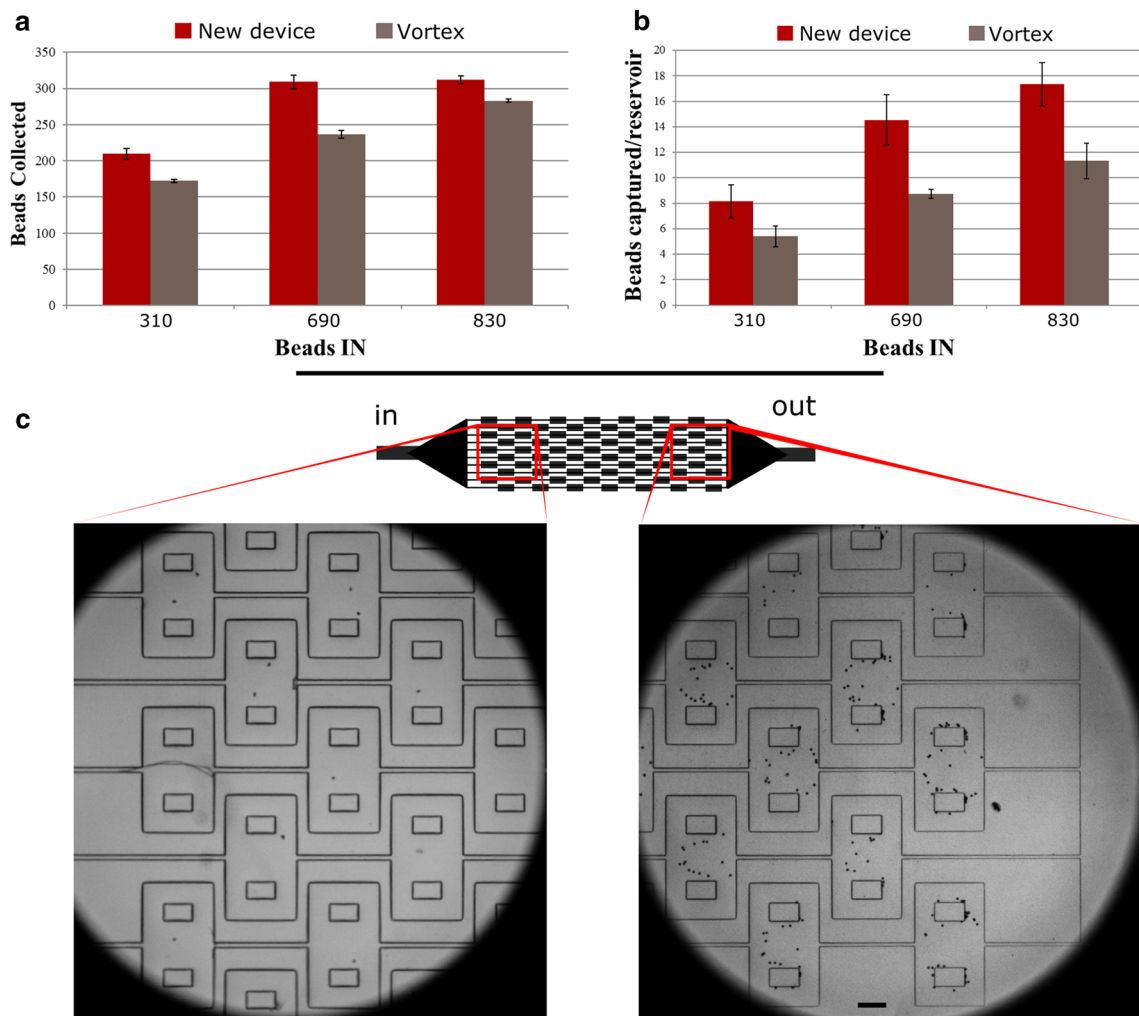


**Fig. 7** Panel a shows the number of captured beads, with the two devices varying the number of processed beads. Note that the new device always presents a higher efficiency with respect to the standard one, even though it seems to saturate earlier. Panel b shows the number of beads captured in the last set of reservoirs along each

channel near the end of the device. Panel c shows two microscope images acquired during the washing step of the same experiment, with the first imaging the reservoirs close to the inlet, and the second the close to the outlet. Scale bar is 200 μm

the Vortex chip, even with a lower efficiency, appears to improve its performance. To better understand this result, we analyzed the video acquired during the washing step of the efficiency test. We noted that the new device efficiency is extremely sensitive to the position of the reservoir in the chip: indeed, the reservoirs located close to the inlet almost capture no beads, while the ones close to the outlet possess a much higher capture efficiency. This is likely due to the deformation of the PDMS substrate that occurs at high flowrate (Sollier et al. 2011), which changes the reservoir geometry and affects the trapping efficiency. Due to pressure drop along the chip this effect is enhanced at the beginning of the chip and almost negligible at the end of it, as shown in Fig. 7c with two microscope images acquired during the washing step. The first picture on the left shows

the reservoirs close to the input where it is possible to note that almost no bead is captured and the reservoir footprint appears deformed; it is important to note the what we see is the expansion of the lateral walls of the reservoirs, while the main bulging occurs in the direction orthogonal to the field of view. On the contrary in the second image, in which the reservoirs are close to the output, no bulging is observed and the reservoirs host many beads. The standard Vortex chip is also affected by the same problem, but it is less deformed, likely due to the lower effective surface area that is affected by the pressurized fluid. On the contrary, the new chip, having reservoirs with a larger area, deforms more under the same stress, limiting the capture efficiency in the first reservoirs more than in the corresponding area of the Vortex chip. Indeed, Gervais et al. (2006) discussed

how in low-aspect-ratio channels (height over width) the bulging effect is not negligible anymore, it increases with the flow rate, and it is proportional to the width of the channel: the larger the channel, the more pronounced will be the height deformation, as expected from our measurements. The PDMS bulging affects the fluid in multiple ways, indeed not only does it introduce a fluid acceleration along the microchannel length (increasing the microchannel height as a function of the inlet proximity), but also due to the local channel deformation it alters the fluid stream lines, the inertial lift force intensity, and the inertial equilibrium position, changing the trapping efficiency. Therefore, the total effect we observe with the new layout is like having a shorter chip, since the bulging experienced is so important that the first reservoirs do not contribute in the trapping, which explains the earlier saturation observed in the new device, with respect to the Vortex chip. To estimate only the effects of the new geometry without being influenced by the bulging of the reservoirs (e.g., similar to what is expected in a rigid chip), we analyzed the videos of the efficiency tests, and the beads captured in the last row of reservoirs only were counted. The last row contains ten pairs of reservoirs, and we further averaged the data over three repeated experiments. Figure 7b shows the number of beads stably trapped per pair of reservoirs, with the two devices, and with varying number of inserted beads. Interestingly, we found out that the new chip captures and stably traps in each reservoir about 1.5 times more beads than the standard one, without showing any saturation effect even between 700 and 800 inserted beads. From these data, we can conclude that the new geometry is extremely promising in increasing the trapping efficiency of the standard Vortex chip. The new geometry can be further enhanced with respect to the 19% increase that we measured, for example by properly choosing the properties of the substrate material. Indeed, a rigid material, like thermoplastic elastomer (TPE) or Norland optical adhesive (NOA) (Sollier et al. 2011), would prevent the bulging effects typical of elastic materials, like PDMS, and make full use of all 12 reservoirs along each channel. Interestingly, using the PDMS device where the trapping of the first five/six reservoirs is completely negligible still allows a 19% increase in the trapping efficiency with the new geometry.

## 5 Conclusions

Vortex technology has been successfully used in size-based sorting of rare cells, being capable of processing the sample in a small amount of time and with good trapping efficiency. Nevertheless, the interparticle interactions is undoubtedly a concern that can limit the device efficiency and makes sample dilution a necessary step. In this work,

we have studied the effects of different reservoirs layouts on the efficiency of vortex-based devices, choosing geometries that facilitate the splitting of the trapped particles into two separate paths, that consist of the unchanged main vortex and a lateral circuit, in order to diminish the particle–particle interactions. We discovered that by properly choosing the lateral fluidic circuit dimension, it is possible to obtain a device which is capable of increasing the efficiency of vortex-based PDMS devices by 19% by combining the increased stability due to the larger reservoir area with the good trapping efficiency of the standard Vortex chip. It is worth mentioning that due to the increased reservoir area a side effect is that we affect the maximum number of reservoirs that can be packed in a single chip, but it is important to stress that this is negligible with respect to the device efficiency, indeed the efficiency we obtain with our standard Vortex device is equal to one presented by Che et al. (2017), with 16 parallel channels instead of the 10 we use. On the contrary we still guarantee high throughput, processing of the sample at 5 ml/min, but combined with an optimized device trapping efficiency which is a major issue when performing CTC isolation. Moreover, we observed that with the new geometry, trapping efficiency is highly dependent on the reservoir position in the chip due to PDMS deformation effects. This permits us to suggest that the new layout efficiency could potentially be further increased with a rigid substrate, which avoids the flow-induced deformation at high flow rates.

### Compliance with ethical standards

**Conflict of interest** The authors declare that they have no conflict of interest.

## References

- Alix-Panabières C, Pantel K (2013) Circulating tumor cells: liquid biopsy of cancer. *Clin Chem* 59:110–118
- Ashworth TR (1869) A case of cancer in which cells similar to those in the tumours were seen in the blood after death. *Aust Med J* 14:146–149
- Bhagat AAS, Hou HW, Li LD et al (2011) Pinched flow coupled shear-modulated inertial microfluidics for high-throughput rare blood cell separation. *Lab Chip* 11:1870–1878
- Che J, Mach AJ, Go DE et al (2013) Microfluidic purification and concentration of malignant pleural effusions for improved molecular and cytomorphological diagnostics. *PLoS ONE* 8:e78194
- Che J, Yu V, Garon EB, Goldman J, Di Carlo D (2017). Biophysical isolation and identification of circulating tumor cells. *Lab Chip*
- Chen J, Li J, Sun Y (2012) Microfluidic approaches for cancer cell detection, characterization, and separation. *Lab Chip* 12:1753–1767
- den Toonder J (2011) Circulating tumor cells: the grand challenge. *Lab Chip* 11:375–377

- Dhar M, Wong J, Karimi A et al (2015) High efficiency vortex trapping of circulating tumor cells. *Biomicrofluidics* 9:064116
- Di Carlo D (2009) Inertial microfluidics. *Lab Chip* 9:3038–3046
- Geislinger TM, Franke T (2013) Sorting of circulating tumor cells (MV3-melanoma) and red blood cells using non-inertial lift. *Biomicrofluidics* 7:044120
- Gervais T, Jamil EA, Axel G, Klavs FJ (2006) Flow-induced deformation of shallow microfluidic channels. *Lab Chip* 6:500–507
- Gupta V, Jafferji I, Garza M et al (2012) ApoStream™, a new dielectrophoretic device for antibody independent isolation and recovery of viable cancer cells from blood. *Biomicrofluidics* 6:024133
- Haddadi H, Di Carlo D (2017) Inertial flow of a dilute suspension over cavities in a microchannel. *J Fluid Mech* 811:436–467
- Hoshino K, Huang YY, Lane N et al (2011) Microchip-based immunomagnetic detection of circulating tumor cells. *Lab Chip* 11:3449–3457
- Kim MS, Sim TS, Kim YJ et al (2012) SSA-MOA: a novel CTC isolation platform using selective size amplification (SSA) and a multi-obstacle architecture (MOA) filter. *Lab Chip* 12:2874–2880
- Lee MG, Shin JH, Bae CY et al (2013) Label-free cancer cell separation from human whole blood using inertial microfluidics at low shear stress. *Anal Chem* 85:6213–6218
- Li P, Stratton ZS, Dao M, Ritz J, Huang TJ (2013) Probing circulating tumor cells in microfluidics. *Lab Chip* 13:602–609
- Lin HK, Zheng S, Williams AJ et al (2010) Portable filter-based microdevice for detection and characterization of circulating tumor cells. *Clin Cancer Res* 16:5011–5018
- Loutherback K, D’Silva J, Liu L et al (2012) Deterministic separation of cancer cells from blood at 10 mL/min. *AIP Adv* 2:042107
- Nagrath S, Sequist LV, Maheswaran S et al (2007) Isolation of rare circulating tumour cells in cancer patients by microchip technology. *Nature* 450:1235–1239
- Ozkumur E, Shah AM, Ciciliano JC et al (2013) Inertial focusing for tumor antigen—dependent and—independent sorting of rare circulating tumor cells. *Sci Transl Med* 5:179
- Pantel K, Alix-Panabières C (2010) Circulating tumour cells in cancer patients: challenges and perspectives. *Trends Mol Med* 16:398–406
- Paris PL, Kobayashi Y, Zhao Q et al (2009) Functional phenotyping and genotyping of circulating tumor cells from patients with castration resistant prostate cancer. *Cancer Lett* 277:164–173
- Pødenphant M, Ashley N, Koprowska K et al. (2015) Separation of cancer cells from white blood cells by pinched flow fractionation. *Lab Chip* 15:4598–4606
- Riethdorf S, Fritsche H, Müller V et al (2007) Detection of circulating tumor cells in peripheral blood of patients with metastatic breast cancer: a validation study of the Cell Search system. *Clin Cancer Res* 13:920–928
- Riethdorf S, Müller V, Zhang L et al (2010) Detection and HER2 expression of circulating tumor cells: prospective monitoring in breast cancer patients treated in the neoadjuvant GeparQuattro trial. *Clin Cancer Res* 16:2634–2645
- Sollier E, Murray C, Maoddi P, Di Carlo D (2011) Rapid prototyping polymers for microfluidic devices and high pressure injections. *Lab Chip* 11:3752–3765
- Sollier E, Go DE, Che J et al (2014) Size-selective collection of circulating tumor cells using vortex technology. *Lab Chip* 14:63–77
- Stott SL, Hsu CH, Tsukrov DI et al (2010) Isolation of circulating tumor cells using a microvortex-generating herringbone-chip. *Proc Natl Acad Sci USA* 107:18392–18397
- Wang X, Papautsky I (2015) Size-based microfluidic multimodal microparticle sorter. *Lab Chip* 15:1350–1359
- Warkiani ME, Guan G, Luan KB et al (2014) Slanted spiral microfluidics for the ultra-fast, label-free isolation of circulating tumor cells. *Lab Chip* 14:28–37
- Yeo T, Tan SJ, Lim CL, et al. (2016) Microfluidic enrichment for the single cell analysis of circulating tumor cells. *Sci Rep* 6:22076
- Zheng S, Lin H, Liu JQ et al (2007) Membrane microfilter device for selective capture, electrolysis and genomic analysis of human circulating tumor cells. *J Chromatogr A* 1162:154–161